

Research Article

Exergy Analysis in Hydrogen-Air Detonation

Abel Rouboa,^{1,2} Valter Silva,¹ and Nuno Couto¹

¹ CITAB/Engineering Department, School of Science and Technology of University of UTAD,
Vila Real 5001-801, Portugal

² MEAM Department, University of Pennsylvania, Philadelphia, PA 19104, USA

Correspondence should be addressed to Valter Silva, vbrsilva@utad.pt

Received 16 December 2011; Accepted 10 April 2012

Academic Editor: Fu-Yun Zhao

Copyright © 2012 Abel Rouboa et al. This is an open access article distributed under the Creative Commons Attribution License, which permits unrestricted use, distribution, and reproduction in any medium, provided the original work is properly cited.

The main goal of this paper is to analyze the exergy losses during the shock and rarefaction wave of hydrogen-air mixture. First, detonation parameters (pressure, temperature, density, and species mass fraction) are calculated for three cases where the hydrogen mass fraction in air is 1.5%, 2.5%, and 5%. Then, exergy efficiency is used as objective criteria of performance evaluation. A two-dimensional computational fluid dynamic code is developed using Finite volume discretization method coupled with implicit scheme for the time discretization (Euler system equations). A seven-species and five-step global reactions mechanism is used. Implicit total variation diminishing (TVD) algorithm, based on Riemann solver, is solved. The typical diagrams of exergy balances of hydrogen detonation in air are calculated for each case. The energy balance shows a successive conversion of kinetic energy, and total enthalpy, however, does not indicate consequent losses. On the other hand, exergy losses increase with the augment of hydrogen concentration in air. It obtained an exergetic efficiency of 77.2%, 73.4% and 69.7% for the hydrogen concentrations of 1.5%, 2.5%, and 5%, respectively.

1. Introduction

The Ramjet propulsion principle was invented at the beginning of the 20th century by Rene Lorin [1, 2], who published it in the technical review "Aérophile" in 1913. A Ramjet is an air-breathing jet engine which uses the engine's forward motion to compress incoming air, without a rotary compressor. The development of this propulsion method was slow and was practically started only from the 1950s. Some years later appeared the pulsed detonation engine (PDE), which is a type of propulsion system that uses detonation waves to combust the fuel and oxidizer mixture [3, 4].

The excitement about pulse detonation engines (PDEs) stems from the fact that, theoretically at least, they can operate at thermal efficiencies about 30% higher than

conventional combustion processes. This is due to the high detonation velocities between $1500 \text{ m}\cdot\text{s}^{-1}$ and $2200 \text{ m}\cdot\text{s}^{-1}$ in a hydrocarbon fuel/air mixture; for example, its thermodynamic cycle is effectively a constant volume or Humphrey cycle [5–7]. The Humphrey cycle can be considered a modification of the Brayton cycle in which the constant-pressure heat addition process of the Brayton cycle is replaced by a constant-volume heat addition process [8].

Due to this thermodynamic efficiency and mechanical simplicity, the PDE technology is more efficient when compared with current engine types. Additionally, the PDE can also provide static thrust for a ramjet or scramjet engine or operate in combination with turbofan systems showing an enormous potential to be applied in many sectors of the aerospace, aeronautic, and military industries. However, there are still engineering challenges that must be overcome, such as to improve methods for initiating the detonation process and develop materials able to withstand with extreme conditions of heat and pressure.

In the PDE technology the combustion takes place in an open-ended tube in which fuel is mixed with air and detonated. As the detonation wave travels down the tube at supersonic speed, a refraction wave propagates into the combustor, and exhaust products leave the chamber. Pressure within the chamber jumps down to charging conditions, which draws in fresh fuel and air, and the cycle is repeated. Each pulse lasts only milliseconds [9, 10]. Detonation is initiated by a predetonator, containing a more readily detonable mixture of fuel air, or by DDT (deflagration detonation transition), a process by which a flame, initiated at the closed end of a duct by a weak spark, accelerates to speeds on the order of $1000 \text{ m}\cdot\text{s}^{-1}$ at which point a detonation wave is initiated within the flame-shock complex [11–13].

The existence of flames for problems with complex chemistry in the combustion approximation has been considered by many authors; see, for example, [14–18]. It has been pointed out in [19], that reaction mechanisms including chain branching can lead to significant qualitative differences in the initiation of detonations in comparison to single step reactions. The use of the exergy concept can be used with advantage to best understand the detonation problem [20]. The exergy gives a quantitative and illustrative description of the convertibility of different energy forms and is a function of the system and environment, whereas entropy is a function only of the system. Total exergy, thermomechanical and chemical, has been defined as the work which can be obtained by taking the system, by means of reversible processes, from its initial state to a state of total equilibrium (dead state), thermal, mechanical, and chemical (“unrestricted equilibrium”), with the environment. This definition entails that the system is in a state of internal equilibrium (uniformity of all intensive properties) and that the environment is in a state which is in internal equilibrium and does not change during time. The exergy of a fluid stream depends upon the choice of the reference environment. This choice, which seems obvious according to some authors [20–22], is, on the contrary, problematic, since every usual environment is a chemical state of nonequilibrium.

A simplified model of adiabatic detonation process in gases was considered by Petela [20] using the concept of exergy. The exergy loss for high pressure shock is larger than that for reactions of combustion. On the other hand, the total exergy loss for deflagration is also larger than that for detonation. Huntchins and Metghalchi [21] analyzing the thermal efficiency show that the Humphrey cycle reveals good advantage compared with Brayton cycle using the same fuel. They also compare the effectiveness of both cycles and conclude that the results using the Humphrey cycle have significant advantage comparing with a Brayton cycle based on the same fuel (methane). Also, the research work of Wintenberger and Shepherd [22] finds that this efficiency cannot be precisely translated into propulsive efficiency. Indeed, the results are only useful in comparing detonations with other combustion modes. They also find that

the efficiency of cycles based on detonation and constant-volume combustion is very similar and superior to a constant-pressure combustion (Brayton) cycle when compared on the basis of pressure at the start of the combustion process.

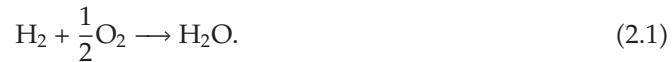
This paper reports an exergy analysis on the detonation wave between the pulse shock wave to the end of the rarefaction wave for various concentrations of the hydrogen in air. Numerical simulation of a two-dimensional detonation of the hydrogen-air mixture is considered. The coupled hydrodynamical model and chemical model integrating the Euler system equations are combined with a detailed chemical reaction model.

2. Numerical Method

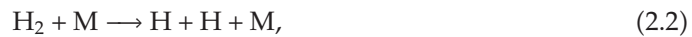
Supersonic combustion, called detonation, occurs coupled to a shock wave traveling at supersonic speed. If premixed gases inside a tube closed at both ends are ignited at one end, a laminar flame first develops, traveling pushed by the expanding hot products behind. The inverted small pressure jump across the flame generates local pressure pulses that wrinkle the flame, create turbulence, extend the burning area, and increase the burning rate, with a positive feedback that, if positively combined with pressure pulses reflected from the other end, might compress the fresh mixture to the autoignition temperature.

2.1. Chemical Model

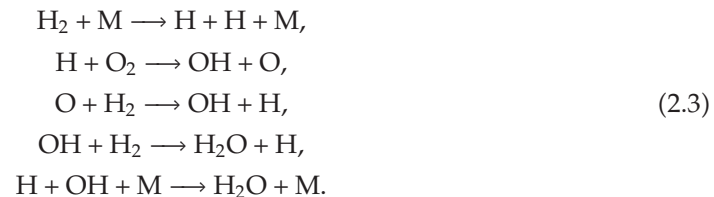
Consider the reaction of hydrogen with oxygen to yield water that is usually written as



The detonation of hydrogen in air must start by dissociation of a hydrogen molecule (it requires less energy than oxygen dissociation):



where M stands for an unspecified molecule (hydrogen, oxygen, a hot wire). The following basic reactions take place:



The chemical kinetic scheme involves seven species, H_2 , O_2 , H_2O , OH , O , H , and N_2 and the above-described 5 elementary reversible reactions. The mechanism is the one proposed by Balakrishnan and Williams [23], and the empirical parameters from each one

Table 1: Empirical values for reactions in the combustion of hydrogen with air [24].

Reaction	A (cm ³ ·gmol) ⁻¹ ·s ⁻¹	b	E_A (MJ·mol ⁻¹)	Temperature range
H + H + M → H ₂ + M	6.4·10 ¹⁷	-1.00	0.0	300–2500 K
H + O ₂ → OH + O	1.2·10 ¹⁷	-0.91	69.1	300–2500 K
O + H ₂ → OH + H	1.5·10 ¹⁷	2.00	31.6	300–2500 K
H + OH + H ₂ O → 2H ₂ O	1.4·10 ²³	-2.00	0.0	1000–3000 K
H ₂ O + M → H + OH + M	1.6·10 ¹⁷	0.00	478.0	2000–5000 K

of the reactions [24] are depicted in Table 1. $k(T, p)$ is the “rate coefficient,” which generally depends on temperature (T), and activation energy and can be defined as follows:

$$k(T) = AT^b e^{-(E_a/RT)}, \quad (2.4)$$

where A is the preexponential factor as in Arrhenius law and E_a is the activation energy. The three parameters A , b , and E_a are determined in practice experimentally.

The chemical production rates are computed using the methodology suggested by Warnatz [25]. In general, for the reaction $A + B \rightarrow$ products not just to species A , it can be defined:

$$\frac{dc_A}{dt} = \frac{dc_B}{dt} = -c_A c_B AT^b \exp\left(\frac{-E_A}{RT}\right). \quad (2.5)$$

2.2. Euler System Equations

The contributions of pressure-driven diffusion, bulk viscosity, and radiative heat transport can be neglected; then the balance equations of mass, momentum, and energy for the two-dimensional unsteady flow for a multicomponent chemically reacting gas mixture are written in the integral form as

$$\begin{aligned} \frac{\partial}{\partial t} \iiint_{\Omega} \rho dV + \iint_{\partial\Omega} \rho (\vec{V} \cdot \vec{n}) dS &= 0, \\ \frac{\partial}{\partial t} \iiint_{\Omega} \rho \vec{V} dV + \iint_{\partial\Omega} (\rho \vec{V} (\vec{V} \cdot \vec{n}) + p \vec{n}) dS &= \vec{0}, \\ \frac{\partial}{\partial t} \iiint_{\Omega} \rho E dV + \iint_{\partial\Omega} (\rho E + p) (\vec{V} \cdot \vec{n}) dS &= 0. \end{aligned} \quad (2.6)$$

The state equation can be defined as follows:

$$p = (\gamma - 1) \cdot \left[\rho E - \frac{1}{2} \rho \vec{V}^2 \right]. \quad (2.7)$$

In these system equations the density $\rho(M, t)$ is the total density of the whole gas in the position M , and at time t . $\rho(M, t)$ is calculated as sum of mass fraction (Y_i) and density (ρ_i) of each species:

$$\rho = \sum_{i=1}^k Y_i \rho_i. \quad (2.8)$$

The above equation system is rewritten in a control volume as follows:

$$\frac{\partial \vec{U}}{\partial t} + \frac{\partial F(\vec{U})}{\partial x} + \frac{\partial G(\vec{U})}{\partial y} = \vec{W}, \quad (2.9)$$

where

$$\vec{U} \equiv \begin{pmatrix} \rho \\ \rho u \\ \rho v \\ \rho E \\ \rho Y_1 \\ \rho Y_2 \\ \vdots \\ \rho Y_{k-1} \end{pmatrix}; \quad \vec{F}(\vec{U}) \equiv \begin{pmatrix} \rho u \\ \rho u^2 + P \\ \rho uv \\ u(\rho E + P) \\ \rho Y_1 u \\ \rho Y_2 u \\ \vdots \\ \rho Y_{k-1} u \end{pmatrix}; \quad \vec{G}(\vec{U}) \equiv \begin{pmatrix} \rho v \\ \rho uv \\ \rho v^2 + P \\ v(\rho E + P) \\ \rho Y_1 v \\ \rho Y_2 v \\ \vdots \\ \rho Y_{k-1} v \end{pmatrix}; \quad \vec{W} \equiv \begin{pmatrix} 0 \\ 0 \\ 0 \\ 0 \\ \dot{w}_1 \\ \dot{w}_2 \\ \vdots \\ \dot{w}_{k-1} \end{pmatrix}. \quad (2.10)$$

In these equations u and v are the velocity vector components in the directions x and y , T the mixture temperature, ρ the mixture density, p the pressure, e and E are the internal and total energies, respectively. For each of the k chemical species, Y_k is the mass fraction, M_k is the molecular, and h_i is the specific enthalpy. Then, the following equations of state can be defined:

$$\begin{aligned} Y_k &= 1 - \sum_{i=1}^{k-1} Y_i, \\ P &= \rho RT \sum_{i=1}^k \frac{Y_i}{M_k}, \\ h_i &= h^0 + \int_{T_0}^T c_{p_i} dT = e_i + \frac{P}{\rho}, \\ E &= e + \frac{1}{2}(u^2 + v^2) = \sum_{i=1}^k Y_i e_i + \frac{1}{2}(u^2 + v^2). \end{aligned} \quad (2.11)$$

2.3. The Solution Procedure

The numerical methods that have been developed in this code for hydrogen and combustion are detailed in [26, 27]. These include lumped parameters, CFD-type codes, and also the

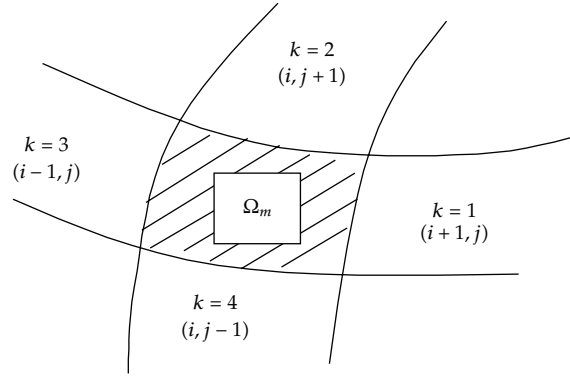


Figure 1: Structured mesh.

CAST3M code [28] developed at the French Atomic Centre Energy (CEA). CAST3M is a general finite-element/finite-volume code for structural and fluid mechanics and heat transfer.

The CAST3M code is used to model both hydrogen dispersion and combustion phenomena over a very wide range of flow regimes, from nearly incompressible flow to compressible flow with shock waves. This could be done by developing a most suitable (i.e., accurate and efficient) numerical method for each type of flow or developing a single method suitable for all flow regimes. We are not aware of any single numerical method able to treat accurately and efficiently flow regimes which range from slowly evolving nearly incompressible buoyant flow to fast transient supersonic flow. However, in practice, for detonation simulation, the use of shock-capturing methods is preferred. In the hydrogen risk analysis tools CEA is developing; the choice was made to develop in the same computational platform CAST3M code for distribution calculations, an efficient pressure-based solver using a semi-implicit incremental projection algorithm which allows the use of “large” time steps, for combustion calculations, a robust and accurate density-based solver using a shock-capturing conservative method.

A brief description of the method we used here, typical for such hyperbolic system equations, follows. Consider the system of hyperbolic conservation laws, (2.10), with the initial conditions:

$$u(x, y, 0) = u_0(x, y). \quad (2.12)$$

Given a uniform grid with time step Δt and spatial mesh size $(\Delta x, \Delta y)$, we define an approximation of U at the point $x_i = i\Delta x, y_j = j\Delta y, tn = n\Delta t$ by the finite volume formula:

$$U_{i,j}^{n+1} = U_{i,j}^{n+1} - \frac{\Delta t}{\Delta x} [F_{i+1/2,j}^n - F_{i-1/2,j}^n] - \frac{\Delta t}{\Delta y} [G_{i,j+1/2}^n - G_{i,j-1/2}^n] + W^n. \quad (2.13)$$

Figure 1 shows the structured mesh used in this problem. Finding the exact solution to the Riemann problem for the equation system (2.9) is complex. Even if we would find it, it would be too complex to use it at each cell boundary, as it needed in (2.13). Therefore, we have to look for some approximate Riemann solver. Here, we adopt the approach described

in [29], which we have already considered in case of conservation laws. Let us rewrite the homogeneous hyperbolic system (2.9) in primitive variables for one direction:

$$\frac{\partial U}{\partial t} + \frac{\partial F(U)}{\partial x} = \frac{\partial U}{\partial t} + A(U) \frac{\partial U}{\partial x} = 0. \tag{2.14}$$

Consider the Riemann problem for (2.14) at each cell boundary $j + 1/2$, that is, with the following initial data:

$$U(x, 0) = \begin{cases} U_j, & x \leq x_{j+1/2} \\ U_{j+1}, & x \geq x_{j+1/2}. \end{cases} \tag{2.15}$$

Following [10, 11], we calculate the Jacobian matrix $A(U)$ in the average state:

$$v_{j+1/2} = \frac{v_j + v_{j+1}}{2}. \tag{2.16}$$

The intermediate state in the solution of the Riemann problem is

$$v_{j+1/2}^* = v_j + \sum_{\lambda_i < 0} a_i r_i, \tag{2.17}$$

where the eigenvalues λ_i and the eigenvectors r_i of the Jacobian matrix $A(v_j + 1/2)$ and a_i are the coefficients of eigenvector decomposition of $(v_j + 1 - v_j)$:

$$v_{j+1/2} - v_j = \sum_{i=0}^6 a_i r_i. \tag{2.18}$$

With the choice of the primitive variables, they are given by the following expressions:

$$\begin{pmatrix} a_0 \\ a_1 \\ a_2 \\ a_3 \\ a_4 \\ a_5 \\ a_6 \end{pmatrix} = \begin{pmatrix} \frac{\Delta_1}{r_{01}} \\ \frac{[-\Delta_3 \rho_a c_a + \Delta_4 + a_0(r_{03} \rho_a c_a - r_{04})]}{2\rho_a c_a^2} \\ \frac{\Delta_2 - a_0 r_{02} - \rho_a(a_1 + a_2)}{[\Delta_3 \rho_a c_a + \Delta_4 - a_0(r_{03} \rho_a c_a + r_{04})]} \\ \frac{[-\Delta_6 \rho_b c_b + \Delta_7 + a_0(r_{06} \rho_b c_b - r_{07})]}{2\rho_b c_b^2} \\ \frac{\Delta_5 - a_0 r_{05} - \rho_b(a_4 + a_6)}{[\Delta_6 \rho_b c_b + \Delta_7 - a_0(r_{06} \rho_b c_b + r_{07})]} \end{pmatrix}, \tag{2.19}$$

where r_{0k} are the components of r_0 and Δk is the k th component of $(v_j + 1 - v_j)$. Recalculating $v_j + 1/2$ into the conservative vector $u_{j+1/2}$, we fully determine the Godunov-type scheme (2.17) for the homogeneous system (2.14).

3. Exergy Calculation

A practical definition of exergy (E) for a closed system is the maximal work that can be obtained when a thermodynamic system is allowed to attain equilibrium with an environment defined as the "dead state," typically defined as the system ambient. If that ambient is at temperature T_0 and pressure, p_0 , the exergy is

$$E = (U - U_0) + p_0(V - V_0) - T_0(S - S_0), \quad (3.1)$$

where U , V , and S denote, respectively, the internal energy, volume, and entropy of the system, and U_0 , V_0 and S_0 are the values of the same properties in the system which were called dead state.

The exergy expression can be generalized considering Q as a heat transfer across a system boundary where the temperature is constant at T_b and taking in account the mass flow across the boundary of a control. The exergy rate balance for a control can be derived using these described approaches, where the control volume forms of mass and energy rate balances are obtained by transforming the closed system forms. The exergy accompanying mass flow and heat transfer can be written as

$$\frac{dE}{dt} = \sum_j \left(1 - \frac{T_0}{T}\right) \cdot Q_j + \sum_{\text{exit}} \dot{m}_e \varepsilon_e - \sum_{\text{inlet}} \dot{m}_i \varepsilon_i, \quad (3.2)$$

where ε_e , ε_i and Q_j are the exit and inlet specific exergy and Q_j is the heat transport rate. The sum of the thermomechanical and chemical exergies is the total exergy associated with a given system at a specified state, relative to a specified exergy reference environment. The chemical exergy is defined as

$$\varepsilon^{ch} = \left(\sum_i n_r \cdot \bar{h}_r - \sum_i n_p \cdot \bar{h}_p \right)_{(T_0, P_0)} - T_0 \left(\sum_i n_r \cdot \bar{S}_r - \sum_i n_p \cdot \bar{S}_p \right)_{(T_0, P_1)} \quad (3.3)$$

or in the following form, when the entropy at (T_0, P_1) is calculated:

$$\varepsilon^{ch} = \left(\sum_i n_r \cdot \bar{h}_r - \sum_i n_p \cdot \bar{h}_p \right)_{(T_0, P_0)} - T_0 \left(\sum_i n_r \cdot \bar{S}_r - \sum_i n_p \cdot \bar{S}_p \right)_{(T_0, P_0)} + RT_0 \ln \left(\frac{\prod_i^{n_r} Y_i}{\prod_i^{n_p} Y_i} \right), \quad (3.4)$$

where Y_r , Y_p , are the mass fraction of reactants and products of involved reactions and h_r , S_r , h_p , and S_p are the specific enthalpy and specific entropy for the reactants and products, respectively. The specific enthalpy terms are determined using the enthalpy of formation for respective substances. The specific entropy appearing in the above equation is absolute entropy. Even if the logarithmic term normally contributes a few percent, it will not be

Table 2: Standard chemical exergies [30].

Species	Standard chemical exergy (kJ·mol ⁻¹)
O ₂	3.900
N ₂	0.640
H ₂ O	8.635
H ₂	235.250

neglected in the present paper. The Gibbs function for each one of the components could be expressed as follows:

$$\varepsilon^{ch} = \left(\sum_i n_r \cdot \bar{g}_r - \sum_i n_p \cdot \bar{g}_p \right) + RT_0 \ln \left(\frac{\prod_i^{n_r} Y_i}{\prod_i^{n_p} Y_i} \right). \quad (3.5)$$

The energy associated with a specific state of a system is the sum of two contributions: the thermomechanical contribution and the chemical contribution. On unit mass, the total exergy is:

$$\varepsilon = \underbrace{(U - U_0) + p_0(V - V_0) - T_0(S - S_0)}_{(1)} + \underbrace{\varepsilon^{ch}}_{(2)} \quad (3.6)$$

where (2.1) is the thermo mechanical contribution and (2.2) is the chemical contribution.

The molar exergy of each reactant and product, at temperature T_1 , is given by

$$\varepsilon_1 = \varepsilon_0 + (\Delta h_{O \rightarrow 1} - T_0 \Delta s_{O \rightarrow 1}). \quad (3.7)$$

The standard chemical exergies of the reactants and products are given in Table 2.

The specific chemical exergy of a material stream is that part of the exergy that results from the sum of the chemical potential differences between the pure reference substances and the pure material stream components at T_0 and P_0 . The specific mixing exergy of a material stream is that part of the exergy resulting from the sum of two contributions.

- (i) The differences in potential between the exergies of the environmental components in environmental concentrations and pure environmental components at T_0 and P_0 .
- (ii) The difference in potential of the exergy due to mixing of the pure components into a mixed material stream at T_0 and P_0 .

The different exergy components are listed in Table 3.

Finally, it can be defined as a "performance factor" the ratio of outlet exergy to inlet exergy:

$$\phi_{\text{eff}} = \frac{\varepsilon_{\text{out}}}{\varepsilon_{\text{in}}}. \quad (3.8)$$

Table 3: Subdivision of the exergy.

Environment	
Change in concentrations of the environment components at T_o and P_o	(Mixture exergy)
Exergy of the pure environment components at T_o and P_o	
Chemical reaction of the pure environment components at T_o and P_o	(Chemical exergy)
Exergy of the pure components at T_o and P_o	
Mixing of the pure components at T_o and P_o	(Mixture exergy)
Change in temperature and pressure at constant composition	
Exergy of the mixed components at T_o and P_o	(Thermo mechanical exergy)
Exergy of the mixed components at T_o and P_o	

4. Results and Discussion

The structure of the pulse detonation and the shock tube is depicted in Figures 2 and 3, respectively.

The detonation field parameters in this work were computed by using the Euler multispecies equations of detonation of H_2 -air mixture. They were solved using the first author's solution procedure [26, 27]. Analyses were carried out for different hydrogen concentrations in air optimum pressure with corresponding temperatures; species concentrations were determined and given first case in figures as function of time. As an example, for first case where the mass fraction of H_2 is equal to 1.5%, peak detonation and end rarefaction density of the selected location were taken at $1.4 \text{ kg}\cdot\text{m}^{-3}$ and $1.1 \text{ kg}\cdot\text{m}^{-3}$, respectively. As a result, optimum shock and rarefaction temperatures were found to be 1930 K and 700 K, respectively. At the same time, the optimum pressures were found to be 18 bar and 6 bar, respectively for the same concentration of hydrogen in air.

As seen in Figure 4 representing the pressure distribution along the tube at 0.003 ms, the optimum pressure at the peak of detonation was found to be 18 bar, 22 bar, and 36 bar for 1.5%, 2.5%, and 5% of hydrogen mass fractions, respectively. Figure 5 shows the result of the temperature at 0.003 ms corresponding to the end of reactions for the case of hydrogen concentration equal to 1.5%. Optimum values vary from 1930 K for the peak of detonation to 700 K for the end of rarefaction. These results show that the structure of the detonation wave is dependent on hydrogen concentration.

Figure 6 shows the shock pressure variation with time for the three different concentrations of hydrogen in air.

The first case considers a hydrogen-air mixture at an initial pressure $P_0 = 1$ bar and initial temperature $T_0 = 298$ K. On the left side of the tube (Figure 3) a pressure pulse (10 bars) is considered to initialize the shock wave. At $t = 0$ s, the shock wave moves from the left to the right side of the tube and initiates the reactions. Shock waves generated due to the formation of a new reaction front are called "reaction shocks" [20]. The reaction shock overtakes the shock front at around $27 \mu\text{s}$, strengthening it and sharply increasing its propagation speed; that is, a detonation wave is formed. Subsequently, the detonation wave speed decreases gradually and a high-frequency, low-amplitude propagation mode is established. In this study no reaction delay is considered, so when the shock wave is initialized, the reactions produced energy. Generally, chemical reactions behind the shock front start generating weak shock waves after approximately $20 \mu\text{s}$ [31]. The plots show the variation in shock front speed with time. Initially the shock wave travels at a constant speed (determined by the

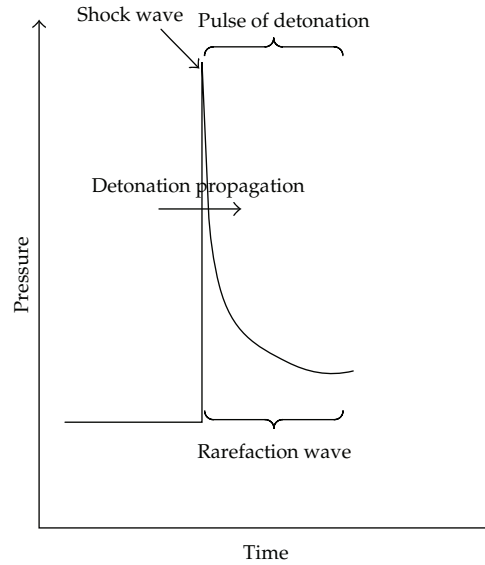


Figure 2: Structure of the pulse detonation.

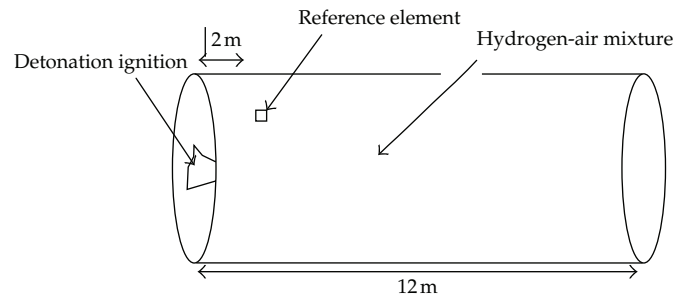


Figure 3: Shock tube.

initial conditions) slightly greater than $1500 \text{ m}\cdot\text{s}^{-1}$, $1800 \text{ m}\cdot\text{s}^{-1}$, and $2200 \text{ m}\cdot\text{s}^{-1}$ for respective hydrogen concentrations of 1.5%, 2.5%, and 5%.

Figures 6 and 7 show the variation with time of pressure and density as function of time and for mass fraction of hydrogen in air: 1.5%, 2.5%, and 5%. As can be seen from these figures, the peak of detonation is characterized by the high-pressure values followed by the rarefaction wave. During the rarefaction wave, the pressure, temperature, and density decrease; this decrease is stopped by the reflected wave from the end of the tube. The most detonation energy is absorbed by the shock when the wave is reflected. This is because by assuming that the detonation is instantaneous and all hydrogen is consumed in the first way of the shock wave, then the energy is completely kinetic, and, as a result, the density and pressure decrease.

Figure 8 shows the mass fraction of H_2O , calculated as function of time for the three studied cases: 1.5%, 2.5%, and 5% of hydrogen concentration. This figure gives us a good idea about mass fraction of H_2O during the detonation for each of hydrogen concentration in air. In fact, the contribution of H_2O in exergy calculation is not negligible since the

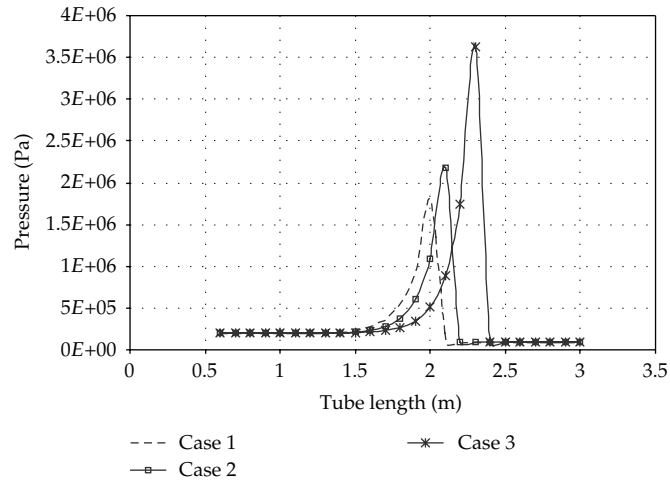


Figure 4: Pressure evolution along shock tube and as function of hydrogen mass fraction in air (case 1: 1.5%, case 2: 2.5%, case 3: 5%).

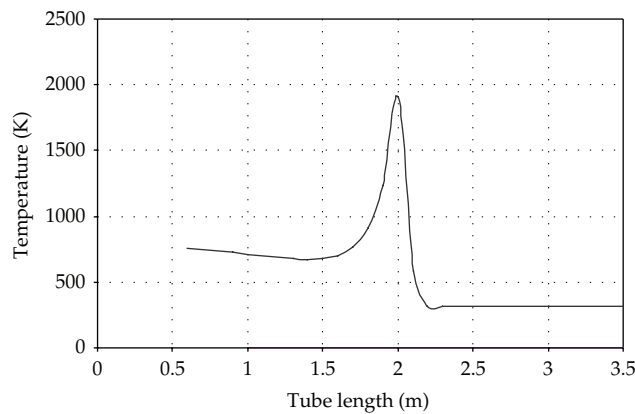


Figure 5: Temperature distribution along the tube length for case 1.

standard chemical exergy of H_2O , O_2 , and N_2 are, respectively, $8.63 \text{ kJ}\cdot\text{mol}^{-1}$, $3.90 \text{ kJ}\cdot\text{mol}^{-1}$, and $0.60 \text{ kJ}\cdot\text{mol}^{-1}$.

Mass fraction for the H_2 , OH , and H_2O system is plotted in Figure 9. Here, the energy levels were chosen to be consistent with those realized in the detonation calculation. As seen in this figure the hydrogen, radical OH , and product H_2O as function of time for the referent element shown on Figure 3, optimum values at the end of reactions, were found to be 0.04%, 0.7%, and 1.2% carried out for species H_2 , OH , and H_2O . These results are presented for the case when the initial mass fraction of hydrogen in air is assumed to be equal to 2.5%.

It is possible to consider the shock and rarefaction processes as the separate successive steps. Therefore, the exergy loss due to the irreversible detonation and the end of rarefaction can be calculated as the product of the initial temperature and the difference between entropies in the start of the shock wave and the end of rarefaction wave. The typical diagrams of exergy balances of hydrogen detonation in air are shown in Figure 10 as function of hydrogen concentration (1.5%, 2.5%, and 5%). Data were calculated for the point of

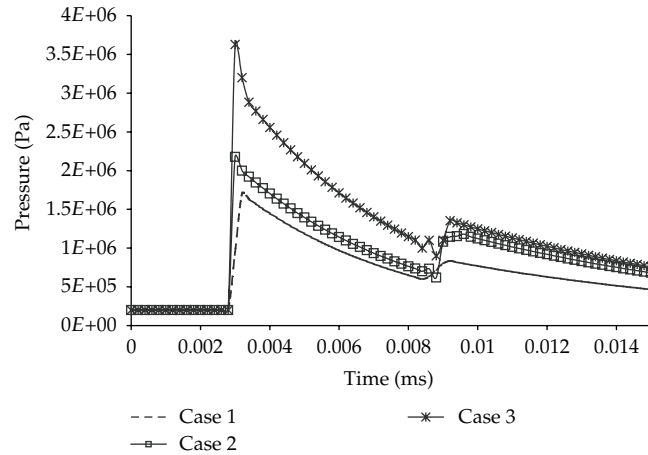


Figure 6: Pressure evolution as function of time with hydrogen mass fraction cases.

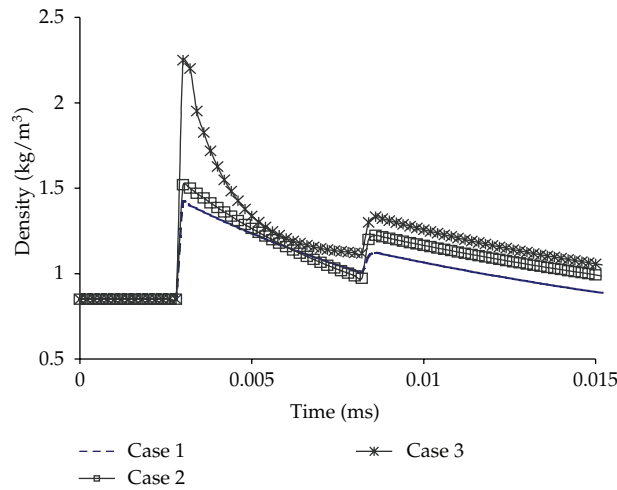


Figure 7: Density evolution for each hydrogen mass fraction in air.

steady detonation. It was shown that exergy losses increase with the augment of hydrogen concentration in air; consequently low hydrogen concentrations in air achieve slight higher efficiencies. It was also verified that the exergy efficiency decreases for all the hydrogen concentrations as a function of the time. It was obtained an exergetic efficiency of 77.2%, 73.4%, and 69.7% for the hydrogen concentrations of 1.5%, 2.5% and 5%, respectively.

On the other hand, the energy balance shows a successive conversion of kinetic energy and total enthalpy, however, does not indicate consequent losses.

5. Conclusions

The CFD code was developed using finite volume discretization method coupled with implicit scheme for the time discretization. The code solves the Euler system equations

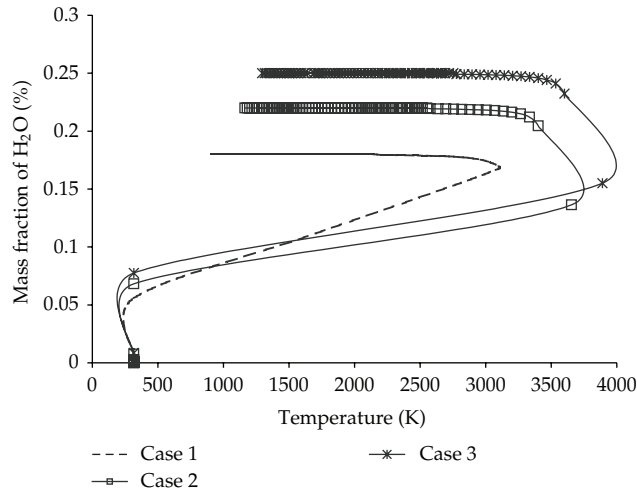


Figure 8: Mass fraction as function of temperature for each hydrogen concentration in air.

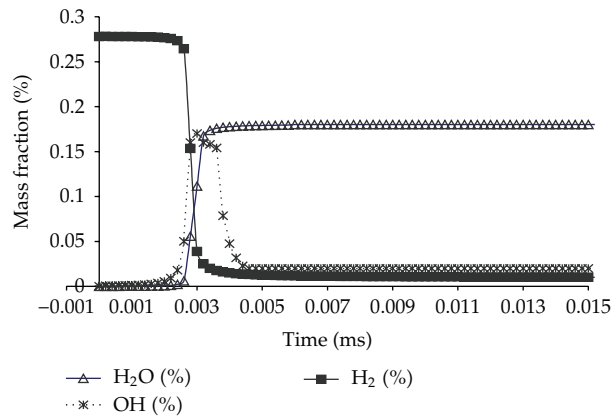


Figure 9: Mass fraction profile of the H₂, OH⁻ and products H₂O.

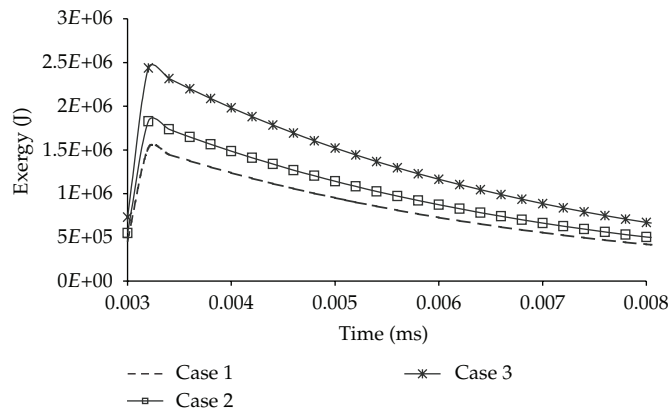


Figure 10: Energy evolution as function of time with hydrogen mass fraction in air.

including a chemistry model, with 5 reactions and 7 species, using an implicit total variation diminishing (TVD) algorithm based on Riemann solver.

There exists a large literature about the numerical discretization of the detonation of hydrogen-air mixture problems: Eulerian schemes, Lagrangian schemes, front tracking techniques, and level set methods, among others. Our main goal, in the present work, is to use detonation parameters, from the beginning to the end of detonation of hydrogen-air mixture to calculate and analyze the exergy loss and the efficiency. The main steps of H₂-air mixture detonation calculation were explained. The developed program is able to calculate the pressure, temperature, density, and mass fraction, for each species from the chemical model. The exergy efficiency was used as objective criteria of performance evaluation.

We conclude in this work that the exergy losses increase with the augment of hydrogen concentration in air, and the efficiency of hydrogen detonation, with low concentration in air, is slightly elevated than the detonation using high hydrogen concentration.

Acknowledgments

The authors would like to express our gratitude to the Portuguese Foundation for Science and Technology (FCT) for the given support to the grant SFRH/BPD/71686 and to the project PTDC/AAC-AMB/103119/2008 and also to The French Atomic Centre Energy (CEA) for all the provided help.

References

- [1] R. S. Fry, "A century of ramjet propulsion technology evolution," *Journal of Propulsion and Power*, vol. 20, no. 1, pp. 27–58, 2004.
- [2] A. Davenas, "History of the development of solid rocket propellant in France," AIAA Paper 93-1785, 1993.
- [3] K. Kailasanath, "Review of propulsion applications of detonation waves," *AIAA Journal*, vol. 39, no. 9, pp. 1698–1708, 2000.
- [4] G. D. Roy, S. M. Frolov, A. A. Borisov, and D. W. Netzer, "Pulse detonation propulsion: challenges, current status, and future perspective," *Progress in Energy and Combustion Science*, vol. 30, no. 6, pp. 545–672, 2004.
- [5] T. Bussing and G. Papas, "An introduction to pulse detonation engines," AIAA Paper 1994-263, 1994.
- [6] S. Eidelman, W. Grossmann, and I. Lottati, "A review of propulsion applications of the pulsed detonation engine concept," AIAA Paper 89-2446, 1989.
- [7] S. Eidelman, W. Grossmann, and I. Lottati, "Air-breathing pulsed detonation engine concept—a numerical study," AIAA Paper 90-2420, 1990.
- [8] W. H. Heiser and D. T. Pratt, "Thermodynamic cycle analysis of pulse detonation engines," *Journal of Propulsion and Power*, vol. 18, no. 1, pp. 68–76, 2002.
- [9] S. Eidelman, I. Lottati, and W. Grossmann, "A parametric study of airbreathing Pulsed Detonation Engine," AIAA Paper 90-2420, 1990.
- [10] A. Wortman, P. Othmer, and W. Rostafinski, "Detonation duct gas generator demonstration program," AIAA Paper 92-3174, 1992.
- [11] S. P. Medvedev, S. V. Khomik, H. Olivier, A. N. Polenov, A. M. Bartenev, and B. E. Gelfand, "Hydrogen detonation and fast deflagration triggered by a turbulent jet of combustion products," *Shock Waves*, vol. 14, no. 3, pp. 193–203, 2005.
- [12] S. P. Medvedev, B. E. Gel'fand, A. N. Polenov, and S. V. Khomik, "Flammability limits for hydrogen-air mixtures in the presence of ultrafine droplets of water (Fog)," *Combustion, Explosion and Shock Waves*, vol. 38, no. 4, pp. 381–386, 2002.
- [13] E. S. Oran, J. W. Weber, E. I. Stefaniw, M. H. Lefebvre, and J. D. Anderson, "A numerical study of a two-dimensional H₂-O₂-Ar detonation using a detailed chemical reaction model," *Combustion and Flame*, vol. 113, no. 1-2, pp. 147–163, 1998.

- [14] H. Berestycki, B. Nicolaenko, and B. Scheurer, "Traveling wave solutions to combustion models and their singular limits," *SIAM Journal on Mathematical Analysis*, vol. 16, no. 6, pp. 1207–1242, 1985.
- [15] A. Bonnet, "Travelling waves for planar flames with complex chemistry reaction network," *Communications on Pure and Applied Mathematics*, vol. 45, no. 10, pp. 1271–1302, 1992.
- [16] P. C. Fife, S. P. Hastings, and C. Lu, "An asymptotic and rigorous study of flames with reversible chain branching," *Asymptotic Analysis*, vol. 5, no. 1, pp. 1–26, 1991.
- [17] S. P. Hastings, C. Lu, and Y. H. Wan, "Existence of a traveling flame front in a model with no cold boundary difficulty," *SIAM Journal on Applied Mathematics*, vol. 47, no. 6, pp. 1229–1240, 1987.
- [18] G. Joulin, A. Liñán, G. S. S. Ludford, N. Peters, and C. Schmidt-Lainé, "Flames with chain-branching/chain-breaking kinetics," *SIAM Journal on Applied Mathematics*, vol. 45, no. 3, pp. 420–434, 1985.
- [19] J. W. Dold and A. K. Kapila, "Comparison between shock initiations of detonation using thermally-sensitive and chain-branching chemical models," *Combustion and Flame*, vol. 85, no. 1-2, pp. 185–194, 1991.
- [20] R. Petela, "Application of exergy analysis to the hydrodynamic theory of detonation in gases," *Fuel Processing Technology*, vol. 67, no. 2, pp. 131–145, 2000.
- [21] T. E. Hutchins and M. Metghalchi, "Energy and exergy analyses of the pulse detonation engine," *Journal of Engineering for Gas Turbines and Power*, vol. 125, no. 4, pp. 1075–1080, 2003.
- [22] E. Wintenberger and J. E. Shepherd, "Thermodynamic analysis of combustion process for propulsion systems," AIAA Paper 2004-1033, 2004.
- [23] G. Balakrishnan and F. A. Williams, "Turbulent combustion regimes for hypersonic propulsion employing hydrogen-air diffusion flames," *Journal of Propulsion and Power*, vol. 10, no. 3, pp. 434–436, 1994.
- [24] D. L. Baulch, C. J. Cobos, R. A. Cox et al., "Evaluated kinetic data for combustion modeling," *Journal of Physical Chemistry*, vol. 21, no. 3, 324 pages, 1992.
- [25] J. Warnatz, *Combustion Chemistry*, Edited by W.C. Gardiner Jr., Springer, New York, NY, USA, 1984.
- [26] A. Rouboa, *Simulation of the detonation of Hydrogen-air Mixture in confined structure*, Ph.D. thesis, University of Paris VI, CEA, (Centre de l'Énergie Atomique a Saclay), 1994.
- [27] A. Rouboa, G. Poissant, A. Forestier, and R. J. Gibert, *Detonation Wave in 2-D Geometry*, vol. 337 of *Fluid-Structure Interaction*, American Society of Mechanical Engineers, Pressure Vessels and Piping Division (Publication) PVP, 1996.
- [28] Castem, "Finite Elements and Finite Volume Code Developed inCEA," Atomic Energy Center, Saclay, France, 2000, <http://www-cast3m.cea.fr/>.
- [29] B. Van Leer, W. Lee, and P. L. Roe, "Characteristic time-stepping or local preconditioning of Euler equations," AIAA Paper 97-1828, 1997.
- [30] M. J. Moran, H. N. Shapiro, D. D. Boettner, and M. B. Bailey, *Fundamentals of Engineering Thermodynamics*, John Wiley & Sons, New York, NY, USA, 7th edition, 2010.
- [31] D. Bradley, C. G. W. Sheppard, I. M. Suardjaja, and R. Woolley, "Fundamentals of high-energy spark ignition with lasers," *Combustion and Flame*, vol. 138, no. 1-2, pp. 55–77, 2004.